Vol 458|5 March 2009|doi:10.1038/nature07816

LETTERS

Temperature-induced A–B intersite charge transfer in an A-site-ordered $LaCu_3Fe_4O_{12}$ perovskite

Y. W. Long[1], N. Hayashi[2], T. Saito[1], M. Azuma[1], S. Muranaka[2] & Y. Shimakawa[1]

Changes of valence states in transition-metal oxides often cause significant changes in their structural and physical properties[1,2]. Chemical doping is the conventional way of modulating these valence states. In ABO_3 perovskite and/or perovskite-like oxides, chemical doping at the A site can introduce holes or electrons at the B site, giving rise to exotic physical properties like high-transition-temperature superconductivity and colossal magnetoresistance[3,4]. When valence-variable transition metals at two different atomic sites are involved simultaneously, we expect to be able to induce charge transfer—and, hence, valence changes—by using a small external stimulus rather than by introducing a doping element. Materials showing this type of charge transfer are very rare, however, and such externally induced valence changes have been observed only under extreme conditions like high pressure[5,6]. Here we report unusual temperature-induced valence changes at the A and B sites in the A-site-ordered double perovskite $LaCu_3Fe_4O_{12}$; the underlying intersite charge transfer is accompanied by considerable changes in the material's structural, magnetic and transport properties. When cooled, the compound shows a first-order, reversible transition at 393 K from $LaCu^{2+}{}_3Fe^{3.75+}{}_4O_{12}$ with $Fe^{3.75+}$ ions at the B site to $LaCu^{3+}{}_3Fe^{3+}{}_4O_{12}$ with rare Cu^{3+} ions at the A site. Intersite charge transfer between the A-site Cu and B-site Fe ions leads to paramagnetism-to-antiferromagnetism and metal-to-insulator isostructural phase transitions. What is more interesting in relation to technological applications is that this above-room-temperature transition is associated with a large negative thermal expansion.

A-site-ordered double perovskites with the general chemical formula $A'A_3B_4O_{12}$ have received much attention owing to their special ordered structures and wide variety of physical properties such as colossal magnetoresistance under weak fields, giant dielectric constant over a wide temperature range and ferrimagnetic transitions above room temperature[7–12]. As shown in Fig. 1, these compounds crystallize with an $Im\bar{3}$ cubic lattice in which the A′- and A-site cations are at the originally 12-fold-coordinated A site in a simple ABO_3 perovskite. Because of the special cation ordering and the heavy tilting of corner-sharing BO_6 octahedra, high pressure is often needed to stabilize the $A'A_3B_4O_{12}$ perovskite structure. Unlike the A site in the simple ABO_3 perovskite, the A site in $A'A_3B_4O_{12}$ accommodates transition-metal ions like Jahn–Teller-distorted Cu^{2+} and Mn^{3+}. Owing to the presence of valence-variable transition-metal ions at both the A site and the B site, $A'A_3B_4O_{12}$ perovskites provide opportunities to study the unusual A–B intersite charge transfer and resultant changes in structural and physical properties.

$LaCu_3Fe_4O_{12}$ prepared at 10 GPa and 1,400 K crystallized as an A-site-ordered double perovskite in which all of the A′ and A sites are respectively occupied by La and Cu ions. (See the high-resolution synchrotron X-ray diffraction (SXRD) pattern at 300 K and the corresponding Rietveld-analysis result in Supplementary Fig. 1.) The oxygen content was proved to be stoichiometric from thermogravimetry (Supplementary Fig. 2). By analogy with other A-site-ordered perovskites like $La/Bi^{3+}Cu^{2+}{}_3(Mn^{3+}Mn^{4+}{}_3)O_{12}$ (refs 10, 13), the nominal composition with oxygen stoichiometry implies a simple ionic formula with a mixed valence at the B site: $La^{3+}Cu^{2+}{}_3(Fe^{3+}Fe^{4+}{}_3)O_{12}$. Bond-valence sum[14] calculations from the result of structure refinement with SXRD data (Supplementary Table 1), however, give valences of +2.90 for Cu ions and +3.05 for Fe ions (Supplementary Table 2). Furthermore, the ^{57}Fe Mössbauer spectrum at room temperature confirms the Fe^{3+} state with a high-spin configuration ($S = 5/2$) as shown in Fig. 2a, where a magnetic sextuplet is seen and the isomer shift of 0.34 mm s^{-1} relative to α-Fe is a typical value for an Fe^{3+} ion in octahedral coordination[15,16]. These results strongly suggest a charge combination of $La^{3+}Cu^{3+}{}_3Fe^{3+}{}_4O_{12}$ at room temperature. We note that the instability of Cu^{3+} ions makes Cu oxides with Cu^{3+} very rare, and it is the high-pressure synthesis of the present compound that stabilizes this unusual high-oxidation state of Cu.

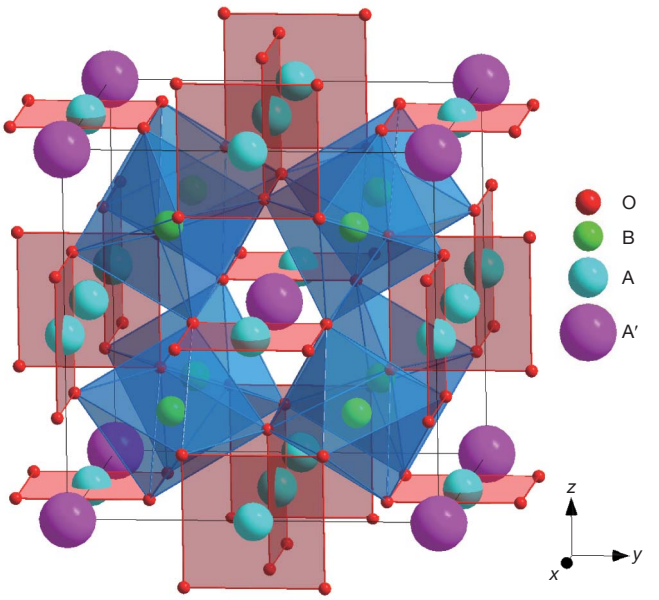

Figure 1 | Crystal structure of the A-site-ordered $A'A_3B_4O_{12}$ double perovskite. The space group is $Im\bar{3}$, and the atomic positions are $2a(0, 0, 0)$, for A′; $6b(0, 0.5, 0.5)$, for A; $8c(0.25, 0.25, 0.25)$, for B and $24g(x, y, 0)$, for O. The A-site ions make square-planar coordinated and isolated AO_4 units and the B-site ions form corner-sharing BO_6 octahedra.

[1]Institute for Chemical Research, Kyoto University, Uji, Kyoto 611-0011, Japan. [2]Graduate School of Human and Environmental Studies, Kyoto University, Sakyo, Kyoto 606-8501, Japan.

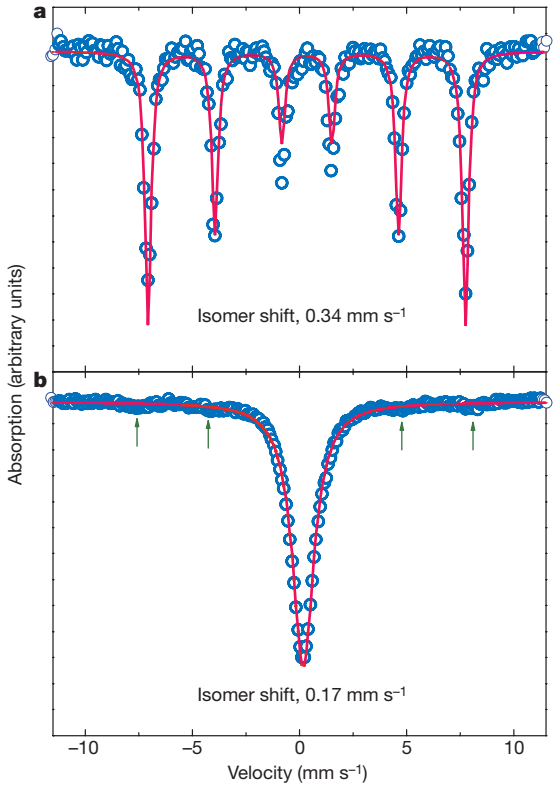

Figure 2 | Temperature dependence of Mössbauer data. **a**, Mössbauer spectrum at room temperature (298 K). **b**, Mössbauer spectrum at 423 K. The solid curves are the fits. The spectrum from a small amount of α-Fe_2O_3 impurity is marked with arrows.

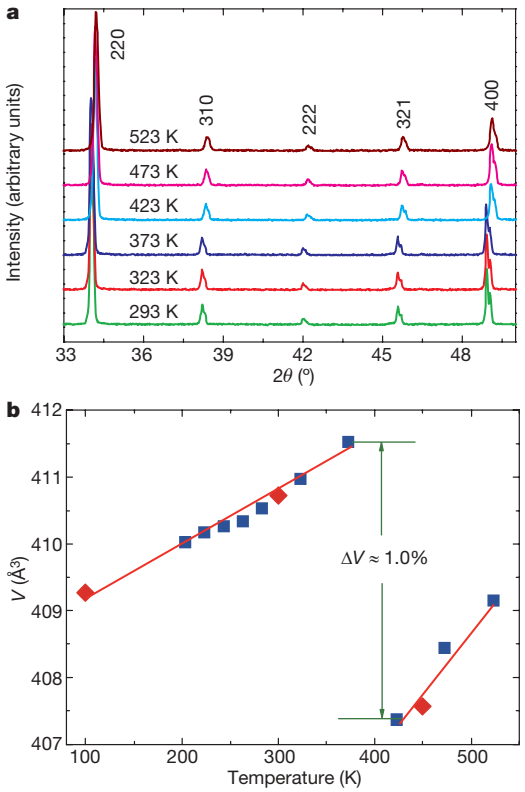

Figure 3 | Anomalous changes in structural data. **a**, Changes in X-ray diffraction patterns with the isostructural phase transition between 373 and 423 K. 2θ, diffraction angle. **b**, Temperature dependence of unit-cell volume, V. The solid lines are guides for the eye. The error bars for the V are smaller than the symbols. The data were obtained from Cu Kα X-ray diffraction (squares) and SXRD (diamonds).

With increasing temperature, the X-ray diffraction patterns of $LaCu_3Fe_4O_{12}$ show the gradual shifts expected from the lattice expansion, but between 373 and 423 K there is an anomalous jump to a larger angle (Fig. 3a). As can be seen in Fig. 3b, the unit-cell volume of $LaCu_3Fe_4O_{12}$ abruptly decreases by ~1.0% around 400 K, which is consistent with the temperature, $T_c = 393$ K, at which a sharp peak was observed in a differential thermal analysis measurement (Supplementary Fig. 2). Because no symmetrical change is discernable, the anomaly at 393 K should be a first-order isostructural phase transition. Moreover, our SXRD measurements confirmed that this transition was completely reversible.

Despite the absence of symmetrical variation in the crystal structure, analysis of the structure of the high-temperature phase revealed notable changes in the bond lengths of both Cu–O in the A-site squares and Fe–O in the B-site octahedra (Supplementary Table 1). The bond-valence sum calculations give valences of +2.06 for the Cu ions and +3.44 for the Fe ions in the high-temperature phase (Supplementary Table 2). In addition, the Mössbauer spectrum at 423 K (Fig. 2b) is very different from that at room temperature. A singlet with an isomer shift of ~0.17 mm s^{-1} suggests an unusual high-oxidation state for Fe ions. Because the typical isomer shifts for Fe^{3+} and Fe^{4+} in octahedral coordination are respectively ~0.35 and 0.07 mm s^{-1} (refs 15–18), the observed isomer shift at 423 K implies that the Fe ions in the present compound are in a valence state intermediate between Fe^{3+} and Fe^{4+}. These results indicate, on the basis of a simple ionic valence calculation, that the high-temperature phase should be $La^{3+}Cu^{2+}{}_3Fe^{3.75+}{}_4O_{12}$. The charge combination above T_c is therefore the same as that of the A-site-ordered perovskites $La^{3+}Cu^{2+}{}_3Mn^{3.75+}{}_4O_{12}$ and $Bi^{3+}Cu^{2+}{}_3Mn^{3.75+}{}_4O_{12}$ (refs 10, 13).

These results strongly suggest that at $T_c = 393$ K there is an unusual charge transfer between the A-site Cu ions and the B-site Fe ions. Simultaneous valence changes ($3Cu^{2+} - 3e^- \rightarrow 3Cu^{3+}$ and $4Fe^{3.75+} + 3e^- \rightarrow 4Fe^{3+}$) lead to the isomorphic phase transition from the high-temperature $LaCu^{2+}{}_3Fe^{3.75+}{}_4O_{12}$ to the low-temperature $LaCu^{3+}{}_3Fe^{3+}{}_4O_{12}$. The unusually high $Fe^{3.75+}$ state instability at low temperature is thus resolved by the A–B intersite charge transfer. This charge transfer contrasts sharply with the charge disproportionation from Fe^{4+} to Fe^{3+} and Fe^{5+} ($2Fe^{4+} \rightarrow Fe^{3+} + Fe^{5+}$) found in an isostructural double perovskite, $CaCu^{2+}{}_3Fe^{4+}{}_4O_{12}$ (ref 19), and a simple perovskite, $CaFe^{4+}O_3$ (ref. 18). In those compounds, the unusual high-valence state Fe^{4+} is stabilized by the disproportionation of charges accompanying a rock-salt-type ordered arrangement of aliovalent species in the ground states. A similar charge disproportionation has been observed even in $Sr_{1-x}La_xFeO_3$ ($x \approx 0.1$–0.6) with an intermediate-valence high-oxidation state Fe (ref. 20). In the present compound, $LaCu_3Fe_4O_{12}$, however, both the X-ray diffraction and Mössbauer spectra confirm the absence of charge disproportionation at temperatures down to 4.2 K. It is interesting that the replacement of the A′-site cation—that is, the substitution of La^{3+} for Ca^{2+} in $CaCu_3Fe_4O_{12}$, which corresponds to substitution at only one-quarter of the A sites in a simple perovskite—leads to the completely different ground state. Again, Cu^{3+} with the square-planar coordination of oxygen ions seldom exists, and this unusual ground state should be stabilized by the special A-site-ordered perovskite structure.

The ilmenite $FeTiO_3$ and the perovskite $BiNiO_3$ are two rare compounds that exhibit an intersite charge transfer, but only under high pressure. The pressure-induced charge transfer in the former is indicated by an irreversible change in Fe^{3+}/Fe^{2+} ratio from ~0.2 to 0.45 (ref. 5). The unusually charge-disproportionated $Bi^{3+}{}_{0.5}Bi^{5+}{}_{0.5}Ni^{2+}O_3$ changes to $Bi^{3+}Ni^{3+}O_3$ at around 4 GPa as a result of the charge transfer from Bi^{5+} to Ni^{2+}, which is accompanied by a structural transition from triclinic to monoclinic[6]. The present A–B intersite charge transfer, by contrast, occurs when temperature changes at ambient pressure and does not change the crystal symmetry. Both $Fe^{3.75+}$ and Cu^{3+} are in

unusually high-valence states that are stabilized by the special ordered crystal structure. Their energy levels should be comparable, and the delicate balance between the two states can be modified by changing temperature. In the A-site-ordered perovskite structure, all oxygen atoms are shared by the FeO_6 octahedra and CuO_4 square-planar units. If the unusual $Fe^{3.75+}$ ($d^{4.25}$) and Cu^{3+} (d^8) high-oxidation states are respectively considered $d^5(Fe^{3+})\underline{L}^{0.75}$ and $d^9(Cu^{2+})\underline{L}$, with ligand holes $\underline{L}$ (ref. 21), the simultaneous valence change should be mediated by 'double charge transfers' between the Fe ions and the O ions and between the Cu ions and the O ions. Thus, the orbital hybridization and correlation effects play a key role in the A–B intersite charge transfer.

The intersite charge transfer gives rise to significant changes in magnetic and transport properties. As seen in Fig. 4a in the temperature dependence of the isomer shift and hyperfine field obtained from the Mössbauer spectrum data, the isomer shift of $\sim$0.17 mm s^{-1} for high-temperature $LaCu^{2+}{}_3Fe^{3.75+}{}_4O_{12}$ abruptly changes to $\sim$0.30 mm s^{-1} at T_c. Correspondingly, a magnetic splitting appears in the Mössbauer spectrum and the hyperfine field increases to $\sim$40 T. These results suggest that for $T < T_c$ there is a magnetic-ordered state due to the Fe^{3+} magnetic species produced by the A–B intersite charge transfer. As shown in the inset of Fig. 4b, the observed linear relationship between magnetization and magnetic field indicates antiferromagnetic ordering below T_c, and a decrease in susceptibility at T_c is consistent with the change from a paramagnetic state to an antiferromagnetic state (Fig. 4b). In the antiferromagnetic $LaCu^{3+}{}_3Fe^{3+}{}_4O_{12}$, Cu^{3+} ions with square-planar coordination are non-magnetic because of the considerable energy splitting between $d_{3z^2-r^2}$ and $d_{x^2-y^2}$ orbitals, as seen in $MCu^{3+}O_2$ (M, alkaline metal), and they do not contribute to the magnetic properties[22,23]. The magnetic ordering is therefore ascribed to the B-site Fe^{3+}–O–Fe^{3+} antiferromagnetic superexchange interactions. This is completely different from the B-site Fe^{3+}–O–Fe^{5+} ferromagnetic coupling in the charge-disproportionated $CaCu_3(Fe^{3+}{}_2Fe^{5+}{}_2)O_{12}$ (ref. 19).

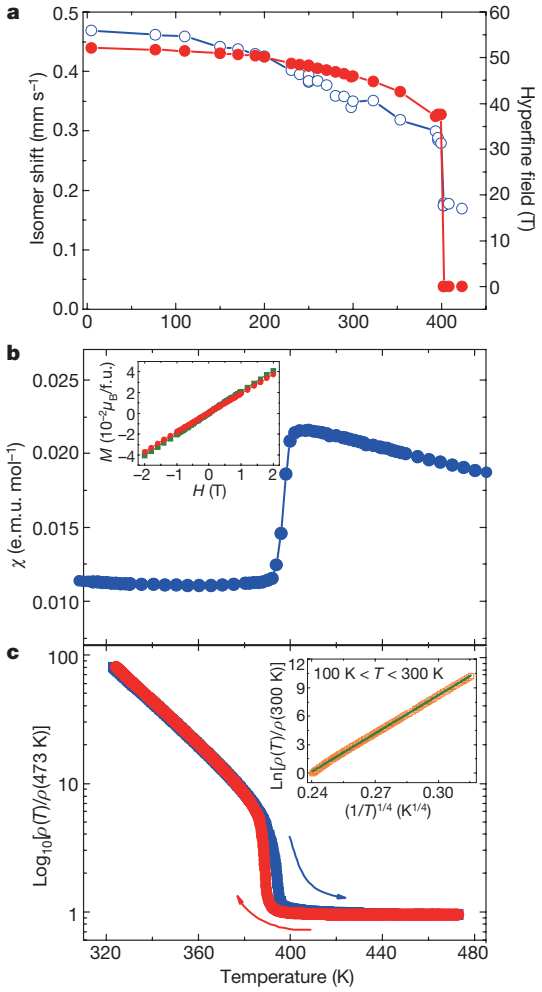

Figure 4 | Temperature dependence of isomer shift and hyperfine field, susceptibility (χ) and normalized resistivity. **a**, The isomer shift (blue) and hyperfine field (red) obtained from the Mössbauer data. **b**, Magnetic susceptibility measured at a magnetic field of $H = 0.1$ T. The inset shows magnetization (M) behaviour at 300 K (circles) and 200 K (squares). μ_B/f.u., Bohr magnetons per formula unit. **c**, Normalized resistivity (ρ). The inset shows the result of fitting to a three-dimensional variable-range hopping model with the formula $\rho(T) = \rho_0 \exp(T_0/T)^{1/4}$.

As seen from the temperature dependence of normalized resistivity (Fig. 4c), the A–B intersite charge transfer also causes a metal-to-insulator transition. The thermal hysteresis and the jump in the resistivity are consistent with the first-order nature of the transition, as shown by the large change in cell volume. Because of the spatial isolation of CuO_4 units (Fig. 1), the electronic configuration of Fe ions dominates the conductivity behaviour. In the high-temperature paramagnetic $LaCu^{2+}{}_3Fe^{3.75+}{}_4O_{12}$ phase, the intermediate valence state of Fe ($d^5\ \underline{L}^{0.75}$) makes the material metallic. In the antiferromagnetic $LaCu^{3+}{}_3Fe^{3+}{}_4O_{12}$ phase, by contrast, a high-resistivity insulating state appears and, as shown in the inset of Fig. 4c, the temperature dependence of resistivity is well fitted by a three-dimensional variable-range hopping model. We emphasize that the observed metal-to-insulator transition caused by the A–B intersite charge transfer in $LaCu_3Fe_4O_{12}$ is essentially different from the resistivity changes induced by the charge disproportionation in the isostructural $CaCu_3Fe_4O_{12}$ and the charge ordering in the isostructural $(NaMn^{3+}{}_3)(Mn^{3+}{}_2Mn^{4+}{}_2)O_{12}$ (refs 19, 24).

We point out that the isotropic volume contraction by as much as $\sim$1.0% that occurs at T_c as temperature increases is a negative thermal expansion (NTE) like that reported in antiperovskite manganese nitrides[25,26]. Materials showing NTE are technologically important, but only a very small number of such materials are known[27]. Furthermore, a characteristic feature of the present charge-transfer-induced NTE in the cubic $LaCu_3Fe_4O_{12}$ is that it is associated with simultaneous transitions in magnetic and electric properties. This implies that the NTE could be controlled by external stimuli such as magnetic field and electric current above room temperature, which would be useful for applications such as elasticity-tuned sensors and switching devices.

METHODS SUMMARY

$LaCu_3Fe_4O_{12}$ was prepared at 10 GPa and 1,400 K with a cubic-anvil-type high-pressure apparatus. The starting materials were La_2O_3, CuO and Fe_2O_3, and $KClO_4$ was used as an oxidizing agent. The residual KCl and a small amount of impurities were washed out using a dilute acid solution. The $LaCu_3Fe_4O_{12}$ structure was studied by X-ray diffraction with Cu Kα radiation and high-resolution SXRD at beamline BL02B2 at Japan's SPring-8 synchrotron facility (wavelength, $\lambda = 0.77747$ Å). The GSAS program was used to refine the structural parameters[28]. ^{57}Fe Mössbauer spectra were obtained using a ^{57}Co/Rh source and a control absorber consisting of α-Fe. The susceptibility and magnetization data were collected with a superconducting quantum interference device magnetometer, and the resistance was measured using a conventional method.

Full Methods and any associated references are available in the online version of the paper at www.nature.com/nature.

Received 17 November 2008; accepted 22 January 2009.

1. Imada, M., Fujimori, A. & Tokura, Y. Metal-insulator transitions. *Rev. Mod. Phys.* **70**, 1039–1263 (1998).
2. Goto, T. & Luthi, B. Charge ordering, charge fluctuations and lattice effects in strongly correlated electron systems. *Adv. Phys.* **52**, 67–118 (2003).
3. Lee, P. A., Nagaosa, N. & Wen, X. G. Doping a Mott insulator: physics of high-temperature superconductivity. *Rev. Mod. Phys.* **78**, 17–85 (2006).
4. Salamon, M. B. & Jaime, M. The physics of manganites: structure and transport. *Rev. Mod. Phys.* **73**, 583–628 (2001).
5. Seda, T. & Hearne, G. R. Pressure induced $Fe^{2+}+Ti^{4+}\rightarrow Fe^{3+}+Ti^{3+}$ intervalence charge transfer and the Fe^{3+}/Fe^{2+} ratio in natural ilmenite ($FeTiO_3$) minerals. *J. Phys. Condens. Matter* **16**, 2707–2718 (2004).

6. Azuma, M. *et al.* Pressure-induced intermetallic valence transition in $BiNiO_3$. *J. Am. Chem. Soc.* **129,** 14433–14436 (2007).
7. Zeng, Z., Greenblatt, M., Subramanian, M. A. & Croft, M. Large low-field magnetoresistance in perovskite-type $CaCu_3Mn_4O_{12}$ without double exchange. *Phys. Rev. Lett.* **82,** 3164–3167 (1999).
8. Subramanian, M. A., Li, D., Duan, N., Reisner, B. A. & Sleight, A. W. High dielectric constant in $ACu_3Ti_4O_{12}$ and $ACu_3Ti_3FeO_{12}$ phases. *J. Solid State Chem.* **151,** 323–325 (2000).
9. Homes, C. C., Vogt, T., Shapiro, S. M., Wakimoto, S. & Ramirez, A. P. Optical response of high-dielectric-constant perovskite-related oxide. *Science* **293,** 673–676 (2001).
10. Takata, K. *et al.* Magnetoresistance and electronic structure of the half-metallic ferrimagnet $BiCu_3Mn_4O_{12}$. *Phys. Rev. B* **76,** 024429 (2007).
11. Sánchez-Benítez, J. *et al.* Preparation, crystal and magnetic structure, and magnetotransport properties of the double perovskite $CaCu_{2.5}Mn_{4.5}O_{12}$. *Chem. Mater.* **15,** 2193–2200 (2003).
12. Shimakawa, Y. A-site-ordered perovskites with intriguing physical properties. *Inorg. Chem.* **47,** 8562–8570 (2008).
13. Alonso, J. A. *et al.* Enhanced magnetoresistance in the complex perovskite $LaCu_3Mn_4O_{12}$. *Appl. Phys. Lett.* **83,** 2623–2625 (2003).
14. Brown, I. D. & Altermatt, D. Bond-valence parameters obtained from a systematic analysis of the Inorganic Crystal Structure Database. *Acta Crystallogr. B* **41,** 244–247 (1985).
15. Li, X. *et al.* Mössbauer spectroscopic study on nanocrystalline $LaFeO_3$ materials. *Hyperfine Interact.* **69,** 851–854 (1991).
16. Blaauw, C. & van der Woude, F. Magnetic and structural properties of $BiFeO_3$. *J. Phys. Chem.* **6,** 1422–1431 (1973).
17. Kawasaki, S., Takano, M. & Takeda, Y. Ferromagnetic properties of $SrFe_{1-x}Co_xO_3$ synthesized under high pressure. *J. Solid State Chem.* **121,** 174–180 (1996).
18. Takano, M. *et al.* Charge disproportionation in $CaFeO_3$ studied with the Mössbauer effect. *Mater. Res. Bull.* **12,** 923–928 (1977).
19. Yamada, I. *et al.* A perovskite containing quadrivalent iron as a charge-disproportionated ferrimagnet. *Angew. Chem. Int. Ed.* **47,** 7032–7035 (2008).
20. Takano, M., Kawachi, J., Nakanishi, N. & Takeda, Y. Valence state of the Fe ions in $Sr_{1-x}La_xFeO_3$. *J. Solid State Chem.* **39,** 75–84 (1981).
21. Bocquet, A. E. *et al.* Electronic structure of $SrFe^{4+}O_3$ and related Fe perovskite oxides. *Phys. Rev. B* **45,** 1561–1570 (1992).
22. Riesemeier, H., Gärtner, S., Lüders, K., Schmalz, M. & Schöllhorn, R. Susceptibility and NQR investigations on $NaCuO_2$. *J. Phys. Chem. Solids* **55,** 613–615 (1994).
23. Imai, K. *et al.* Preparation, crystal structure, and magnetic property of a new compound $LiCuO_2$. *J. Phys. Soc. Jpn* **61,** 1819–1820 (1992).
24. Prodi, A. *et al.* Charge, orbital and spin ordering phenomena in the mixed valence manganite $(NaMn^{3+}{}_3)(Mn^{3+}{}_2Mn^{4+}{}_2)O_{12}$. *Nature Mater.* **3,** 48–52 (2004).
25. Takenaka, K. & Takagi, H. Giant negative thermal expansion in Ge-doped anti-perovskite manganese nitrides. *Appl. Phys. Lett.* **87,** 261902 (2005).
26. Takenaka, K., Asano, K., Misawa, M. & Takagi, H. Negative thermal expansion in Ge-free antiperovskite manganese nitrides: Tin-doping effect. *Appl. Phys. Lett.* **92,** 011927 (2008).
27. Sleight, A. W. Isotropic negative thermal expansion. *Annu. Rev. Mater. Sci.* **28,** 29–43 (1998).
28. Larson, A. C. & von Dreele, R. B. *General Structure Analysis System (GSAS)*. Report No. LAUR 86-748 (Los Alamos National Laboratory, 1994).

Supplementary Information is linked to the online version of the paper at www.nature.com/nature.

Acknowledgements We thank K. Nishimura and K. Oka for help with the high-pressure synthesis and magnetic measurements, and we thank K. Jungeun for help with the SXRD experiments. Thanks are also due to M. Takano for discussions. This work was partly supported by Grants-in-Aid for Scientific Research (19GS0207, 18350097, 17038014, 19014010 and 19340098), by the Global COE Program 'International Center for Integrated Research and Advanced Education in Materials Science' and by a grant for the Joint Project of Chemical Synthesis Core Research Institutions from the Ministry of Education, Culture, Sports, Science and Technology of Japan.

Author Contributions Y.W.L. and Y.S. designed the study; Y.W.L. synthesized the sample and performed X-ray diffraction, thermogravimetric, magnetic and electrical measurements with the help of M.A. and T.S.; N.H. carried out Mössbauer measurements with the help of S.M.; all of the authors discussed the results; and Y.W.L. and Y.S. wrote the manuscript.

Author Information Reprints and permissions information is available at www.nature.com/reprints. Correspondence and requests for materials should be addressed to Y.W.L. (ywlong@msk.kuicr.kyoto-u.ac.jp) or Y.S. (shimak@scl.kyoto-u.ac.jp).

METHODS

Raw oxide materials La_2O_3, CuO and Fe_2O_3 in the mole ratio 1:6:4 were used to prepare the A-site-ordered perovskite $LaCu_3Fe_4O_{12}$. The mixture of the starting materials was put into a platinum capsule with an oxidizing agent ($KClO_4$) and was treated at 10 GPa and 1,400 K for 1 h with a cubic-anvil-type high-pressure apparatus. The residual KCl and a small amount of unreacted reagents were washed from the product using dilute acid.

The high-resolution SXRD was performed with the large Debye–Scherrer camera with an imaging plate detector installed at beamline BL02B2 at SPring-8. The powder sample was put into a glass capillary tube with an inner diameter of 0.1 mm and was rotated during the measurements. The wavelength used was 0.77747 Å. The SXRD data were collected at 100, 300 and 450 K in a 2θ range from 1° to 75° with a 0.01° resolution and were analysed by the Rietveld method using the GSAS software[28]. Conventional X-ray diffraction was performed, using a Rigaku X-ray diffractometer, with Cu Kα radiation (40 kV, 300 mA) at temperatures from 173 to 523 K to see changes in the lattice parameters and the phase transition.

Thermogravimetric measurements were made, using a Rigaku TG-DTA 8120 system, from room temperature to 1,200 K in air with a heating rate of 10 K min^{-1}. The oxide products of $LaCu_3Fe_4O_{12}$ decomposition were identified by X-ray diffraction. The ^{57}Fe Mössbauer spectra were obtained in transmission geometry using a ^{57}Co/Rh γ-ray source in combination with a constant-acceleration spectrometer. The source velocity was calibrated by using pure α-Fe. The obtained spectra were fitted by a least-squares method with Lorentzian functions. Magnetic susceptibility and magnetization were measured using a Quantum Design superconducting quantum interference device magnetometer in a zero-field cooling mode. The susceptibility measurements were made at 0.1 T in the temperature range from 5 to 500 K. The magnetization in the magnetic ordered state was measured at 200 and 300 K under field strengths between -2 and 2 T. The electrical resistance of the sample was measured using a conventional four-probe method. Thermal hysteresis of the resistance around the transition temperature was measured while heating and cooling at 0.5 K min^{-1}.